Hydrogen evolution by a photoelectrochemical cell based on a Cu_2O-ZnO-[FeFe] hydrogenase electrode

Lei Tian[1, †], Brigitta Németh[2, †], Gustav Berggren[2,*], Haining Tian[1,*]

1. *Physical Chemistry, Department of Chemistry – Ångström Laboratory, Uppsala University, BOX 523, 75120, Uppsala, Sweden. E-mail: haining.tian@kemi.uu.se*
2. *Molecular Biomimetics, Department of Chemistry – Ångström Laboratory, Uppsala University, BOX 523, 75120, Uppsala, Sweden. E-mail: gustav.berggren@kemi.uu.se*

† These authors contribute equally

Abstract

A Cu_2O-ZnO-hydrogenase photocathode possessed enzyme/semiconductor junction has been constructed by immobilizing a biological protein catalyst, hydrogenase-CrHydA1 enzyme on the ZnO protected Cu_2O electrode. With light illumination, a photocurrent of 0.8 mA/cm^2 at 0.15 V *vs.* RHE was obtained and hydrogen was successfully detected from the photocathode in photoelectrochemical measurements with Faradaic efficiency of ca. 1%. The construction as well as the stability of the system are also reported. The result shows that this biohybrid photocathode is capable of photocatalytic proton reduction under mild conditions.

Keywords: Photocathode, Water splitting, Copper (I) oxide, Hydrogenase, Photoelectrochemical cell

1. Introduction

Photoelectrochemical (PEC) Cells [1-3] is a promising technique for storage of solar energy in the form of high energy chemical bonds, *via* e.g. CO_2 reduction into carbonate fuels[4] or water splitting into H_2 and O_2[5]. Two main requirements have to be considered to achieve satisfactory performance in PEC: 1) high-performance photoelectrodes, including photoanodes and photocathodes; 2) effective catalysts to minimize energy losses during chemical conversion. Molecular PEC devices are normally constructed by wide band gap semiconductor electrodes, e.g. TiO_2[6] and NiO[7-8]. Light absorber dye molecules and molecular catalysts, have attracted intense interest due to the facile modification of molecules for device optimization. Molecular photoanodes, responsible for the oxidation reaction in PEC cell, have obtained higher energy conversion efficiency than those reported for molecular photocathodes so far[9]. Conversely, progress on such photocathodes is limited by a few suitable p-type semiconductors and efficient catalysts[7, 10-11]. Another strategy is to apply the semiconductors with narrow band gap (e.g. α-Fe_2O_3[12] and $BiVO_4$[13] in the photoanodes; p-Si[9] and InP[14] in the photocathodes) as the direct visible light absorber instead of dye sensitized large band gap semiconductor electrodes. Still, the research on the photocathode side is rather limited compared to the photoanode side because of the complicated preparation process and instability of those p-type semiconductors commonly utilized[9, 14]. Thus, further development of the photocathode is required in order to construct an efficient and complete tandem PEC for over-all water splitting.

Cu_2O is a rare example of a naturally conductive p-type semiconductor material. It possesses a suitable band gap (2.1 eV) for absorption of visible light, and its conduction and valance bands are suitable for proton reduction and water oxidation with driving forces of 0.7 V and 0.17 V, respectively. Critically, calculation estimates support the potential of this material as a high-performance photocathode in PEC cell applications since a theoretical photocurrent of 14.7 mA/cm^2 and a photon to H_2 conversion

efficiency of 18 % can be obtained from Cu_2O[2]. The main drawback of Cu_2O in the H_2 evolution reaction (HER) is its instability, as the application of a bias potential and light causes the reduction of Cu_2O into metallic Cu in the presence of water. However, this stability issue can be addressed by importing a band gap matched n-type semiconductor on top of Cu_2O to construct a heterojunction structure[15-16]. Therefore, in this work, we chose Cu_2O as p-type light absorbing semiconductor and used n-type ZnO semiconductor to protect Cu_2O layer. Also, as Cu_2O and ZnO can form good p-n junction structure due to well-matched conduction and valence band positions, allowing photo-generated electrons in Cu_2O can flow to ZnO layer.

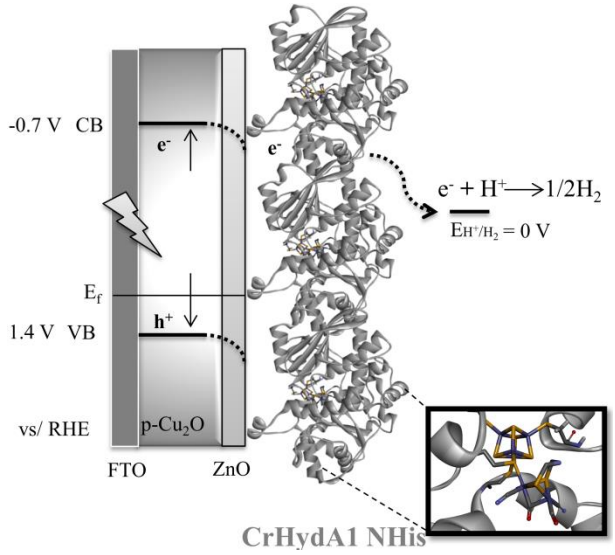

Scheme 1. representation of the Cu_2O-ZnO-hydrogenase photocathode. The active site of the [FeFe] hydrogenase shown in inset (structure based on the CpI hydrogenase, PBD ID number: 3C8Y; color coding: light blue-nitrogen, dark-blue iron, golden-sulfur, red-oxygen, dark grey-carbon, light gray ribbon-protein backbone); CB: conduction band; VB: valence band; E_f: the Fermi level; all the potentials are based on Reversible Hydrogen Electrode (RHE).

ZnO is not a proton reduction catalyst; therefore, a real and good catalyst was required for the electrode to reduce the HER potential barrier, i.e. to shift the onset catalytic potential to more positive range. Previous studies have successfully employed e.g. Pt [2], RuO_x [17] NiMo [18] and CoMo [15], as proton reduction catalysts. In order to replace catalysts based on noble and/or toxic metals elements, while retaining satisfactory catalytic performance, we explored the hydrogenase enzyme as the hydrogen evolution catalyst. These biological systems are the most efficient molecular catalysts for H^+/H_2 interconversion to date and capable of operating at neutral pH with minimal over-potentials.[19] Importantly, the possibility to employ such enzymes in other (photo-) electrochemical applications *via* surface immobilization have already been verified [9, 20-24]. More specifically, we employed the [FeFe] hydrogenase from *Chlamydomonas reinhardtii* (CrHydA1), to construct Cu_2O-ZnO-hydrogenase photocathode shown in Scheme 1. Herein we describe the construction as well as the stability of the system, and show that this biohybrid photocathode was capable of photocatalytic proton reduction under mild conditions.

2. Experimental

2.1. General

All chemicals were purchased from Sigma-Aldrich or VWR and used as received unless otherwise stated. Protein content was analyzed by 12% SDS-PAGE minigels in a SE250 Mighty Small II unit (Hoefer) system. The proteins were stained with Page Blue protein staining solution (Thermo Fisher Scientific) according to the supplier's instructions. All anaerobic work was performed in an MBRAUN glovebox ($[O_2]$ < 10 ppm). The expression vectors coding the *csdA* and *hydA1* genes were kindly provided by Prof. Marc Fontecave (College de France, Paris/CEA, Grenoble). The His-tagged CsdA enzyme was purified following a literature procedure.[25] $(Et_4N)_2[Fe_2(adt)(CO)_4(CN)_2]$, adt = $^-SCH_2NHCH_2S^-$) was synthesized in accordance to literature protocols with minor modifications, and verified by FTIR spectroscopy.[26]

2.2. The hydrogenase sample preparation

The his-tagged CrHydA1 enzyme was heterologous expressed in *E.coli* BL21(DE3) and reconstituted in vitro following a literature procedure with minor modifications.[27-29] The quality of the enzyme preparations were verified by EPR and UV/Vis spectroscopy as well as a chemical enzyme activity assay. The holo-hydrogenase enzyme preparations were aliqouted, flash frozen and kept at -80 °C until further use. Detailed protocols can be found in Supporting Information (SI).

2.3. Preparation of Cu_2O electrode

The Cu_2O electrode was prepared by electrodeposition method from an alkaline solution of lactate-stabilized copper sulphate according to the reported method[30]. Cu_2O electrodeposition in this work was performed directly on the fluorine doped tin oxide (FTO) glass. Briefly, FTO glass was dipped into 0.2 M $CuSO_4$ and 3 M lactic acid in deionized water solution at pH 12 adjusted by 2 M K_2HPO_4 buffer. The electrodeposition was under a constant current density of 0.1 mA/cm^2 for 10600 s, performed by a two-electrode deposition method. The temperature of electrolyte bath was maintained at 30 °C.

2.4. Preparation of Cu_2O-ZnO electrode

100 μL ZnO precursor solution with 0.5 M zinc acetate dehydrate and 0.5 M ethanolamine in 2-ethoxyethanol solvent was spin-coated on the previously prepared Cu_2O electrode (20 mm ×10 mm) with a speed of 2000 rpm for 30 s. The spin-coating process was repeated by three times. Subsequently, the electrode was annealed at 220 °C under ambient atmosphere for 30 min to form the Cu_2O-ZnO electrode.

2.5. Preparation of Cu_2O-ZnO-hydrogenase photoelectrode

The Cu_2O-ZnO electrode was covered by insulating black tape with a 0.25 cm^2 exposed active area. A 70 μM stock solution of hydrogenase in 100 mM phosphate buffer (pH 6.8) was prepared immediately prior to the electrode preparation. Then, 5 μL of hydrogenase stock solution was drop casted uniformly onto the active area of the Cu_2O-ZnO electrode, and dried for 15 min. The resulting Cu_2O-ZnO-hydrogenase photocathode, Ag/AgCl (in saturated KCl) reference electrode and Pt counter electrode was assembled into a well-sealed "HT-PEC" holder (Dyenamo AB), and 100 mM phosphate buffer (pH 6.8) was injected into the holder as electrolyte for subsequent PEC tests. The whole procedure above was performed under strict anaerobic conditions. The light illuminated from back side of the photocathode.

2.6. PEC tests

The PEC response was tested by linear sweep voltammetry (LSV) with the "HT-PEC" setup, utilizing AUTOLAB potentiostat with three-electrode configuration. A LED PAR38 module (17 W, 5000K, Zenaro Lighting GmbH, 420-750 nm) was used as the light source during all the PEC tests. The light intensity of the LED lamp is similar to the light intensity of visible light region in standard 1 Sun. The active area is determined to 0.25 cm^2 by a black tape mask mentioned before. All the potentials were converted into RHE based by the equation: $E_{RHE} = E_{(Ag/AgCl)SHE} + 0.059pH + E_{(Ag/AgCl)}$[31].

2.7. Hydrogen evolution test

The hydrogen evolution measurement was performed by chronoamperometry method assisted by a 0 V *vs*. RHE bias potential. The production of hydrogen was detected by a pre-calibrated Unisense microsensor setup.

2.8. Structural and optical characterization

Cu_2O electrode, Cu_2O-ZnO electrode before and after hydrogen evolution measurement, and Cu_2O-ZnO-hydrogenase photocathode after the hydrogen evolution test were denominated as Cu_2O, Cu_2O-ZnO-b, Cu_2O-ZnO-a and Cu_2O-ZnO-hydrogenase-a, respectively. The SEM images were taken by a Leo 1550 FEG microscope (Zeiss, Oberjochen, Germany), and elements mapping analysis was measured with an 80 mm^2 Silicon Drift EDX detector. Small angle-X-ray diffraction patterns were acquired by Siemens D5000.

2.9. ZnO binding test

The binding of CrHydA1 to ZnO was verified by a chemical enzymatic assay, performed in 100 mM potassium phosphate buffer in 200 µl final volume. A 100 µl stock 70 µM solution of the hydrogenase enzyme was mixed with 100 µl 60 mg/ml ZnO suspension. The suspension was incubated for 5 minutes at room temperature and then centrifuged for 1 minute at 13.000 rpm; the supernatant was separated to remove any unbound protein (sample flowthrough (FT)). The remaining pellet was washed twice by re-suspending it in 200 µl phosphate buffer followed by centrifugation, to remove any residual weakly bound enzyme from the pellet (the resulting supernatant: wash1 (W1) and wash2 (W2)). The washing steps were followed by an elution step in which the pellet was re-suspended in 200 µl phosphate buffer with 500 mM imidazole and centrifuged again (the resulting supernatant: elution (E)). The final pellet was re-suspended in 200 µl phosphate buffer (re-suspended pellet (P)).

To estimate the binding capacity, 20 µl from each fraction was used in a chemical hydrogen evolution assay performed as described in the SI. 20 µl of the initial hydrogenase stock solution was used for a positive control and represented 100% of the possible enzymatic activity.

The binding was also verified by SDS-PAGE gels by studying the CrHydA1 band (49 kDa). The ZnO binding test was repeated, but the different fractions were combined with 4x SDS-PAGE loading buffer, boiled for 15 minutes at 95 °C until the volume was reduced under 30 µl and the protein samples were loaded onto 12 % SDS-PAGE gel.

3. Results and discussion

3.1 Preparation, morphology and crystal structure of the Cu_2O and Cu_2O-ZnO electrodes

Cu_2O as a p-type semiconductor has potential for application in HER due to its suitable band gap (2.1 eV) and conduction band position (0.7 V negative to the potential of H^+/H_2). However, its instability especially when exposed to H_2O and light restricts its application as photocathode in PEC. A common

strategy for addressing this instability is to deposit a protective semiconductor layer on the surface of Cu_2O. Previously, this layer has been generated by Atomic Layer Deposition (ALD)[2] or thermal evaporation[15] methods. In this study we prepared the Cu_2O electrode by electrodeposition on an FTO support (denoted Cu_2O-b). The ZnO protection layer was then deposited by the spin-coating method (denoted Cu_2O-ZnO-b). In order to gain insight into the morphology of the Cu_2O and Cu_2O-ZnO-b electrodes, Scanning Electron Microscopy (SEM) was employed. The corresponding images are shown in Figure 1a and 1b. A planar film structure with several micrometers of grain size and zigzag morphology was observed in Cu_2O-b electrode. When a ZnO layer was coated onto the Cu_2O-b surface (Figure 1b) to generate Cu_2O-ZnO-b, the boundary between the Cu_2O grains became obscured, which is significantly different from the pure Cu_2O-b sample (Figure 1a). Also, the color of the Cu_2O-b turned more dark red after the ZnO layer was deposited (inset in Figure 1a and 1b). The result suggests that there is uniform coating of the ZnO layer in the Cu_2O-ZnO-b electrode.

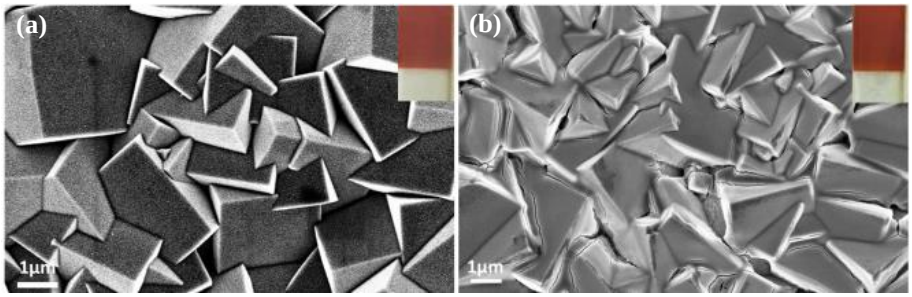

Figure 1. the SEM morphology and the appearance inserted in upper right corner of the photoelectrodes. a) Cu_2O, b) Cu_2O-ZnO-b.

Upon small-angle X-ray diffraction (XRD) tests (Figure 2), polycrystalline Cu_2O structure was confirmed along with a main (111) orientation peak. The (111) oriented grains lead to cubic structure with the exposed {100} faces[30], which is consistent with the result of SEM. No XRD peaks can be ascribed to the formation of crystallized ZnO, indicating that the ZnO coating layer on Cu_2O surface is amorphous structure.

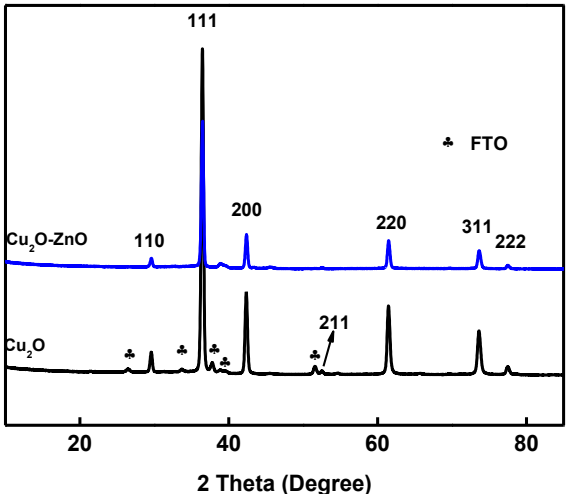

Figure 2. Small-angle X-ray diffraction curves of Cu_2O-ZnO (top) and Cu_2O (bottom).

3.2 Light response of the photoelectrodes

According to the previous reports[2, 30], bare Cu_2O electrode also has light response in the presence of water, contributing photocurrent in a PEC device. However, the produced photocurrent is not used for proton reduction, but for decomposition of Cu_2O material into metallic Cu, which is an unwanted reaction in our system. Therefore, we employed a layer of ZnO on top of Cu_2O layer to prevent Cu_2O from interacting with water phase. In principle, we should observe significantly decreased photocurrent in Cu_2O-ZnO-b electrode in comparison to that of bare Cu_2O-b electrode. To verify this, Cu_2O-b and Cu_2O-ZnO-b electrodes were tested by linear scanning voltammetry (LSV) test with the chopped light, in which the photocurrent and dark current can be simultaneously monitored (Figure S1). An obvious light response was observed during the first scan of the LSV test of the Cu_2O-b electrode. Moreover, the electrode lost its original red Cu_2O color and turned black due to the formation of Cu after 1st LSV scanning. However, no H_2 was detected from PEC test of Cu_2O-b electrode, implying that all photocurrent generated was used for decomposition of Cu_2O material or other side reactions (see Figure S6a) instead of proton reduction. From 2nd LSV scanning, the photocurrent decreased significantly and the dark current was observed probably due to formation of Cu which could be an efficient catalyst for electrocatalytic proton reduction or side reactions.

Conversely, when a ZnO layer was deposited onto Cu_2O, the resulting Cu_2O-ZnO-b system showed much less photocurrent than that from bare Cu_2O-b electrode. Moreover, the photocurrent is relatively stable for several scans. Although, a photocurrent of 80 $\mu A/cm^2$ at 0.15 V *vs.* RHE was generated in Cu_2O-ZnO-b electrode, there is still no hydrogen detected in this system. We tentatively attribute the low photocurrent to the reduction of an unknown species in the electrolyte or a slow degradation of the electrode. In summary, these results suggest that the Cu_2O material was well protected by ZnO layer.

3.3 Verification of the Cu_2O-ZnO-hydrogenase electrode

The low photocurrents observed for the Cu_2O-ZnO electrode combined with its apparent stability suggest that introduction of a suitable catalyst could improve the performance of this photocathode. To test this we explored the possibility of functionalizing the surface with the CrHydA1 enzyme, because of its low overpotential and high performance in HER. The capacity of the enzyme to bind with ZnO particles and the influence of immobilization on its catalytic properties was verified *via* a binding test in combination with enzymatic assays and protein visualization by SDS-page gel.

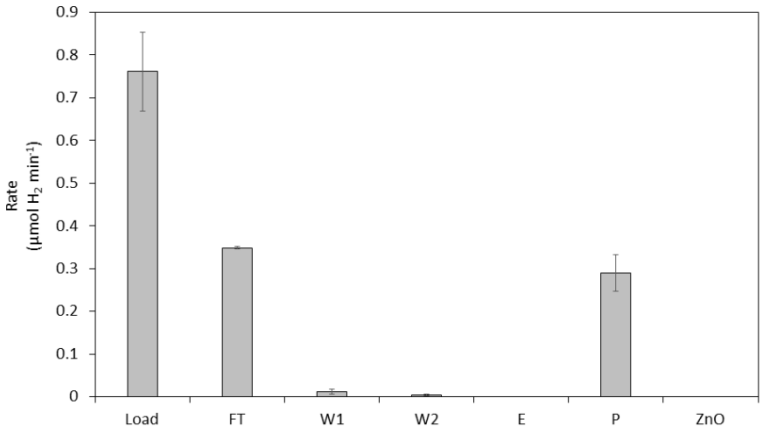

Figure 3. The adsorption of CrHydA1 to ZnO particles in hydrogen evolution capacity of the different fractions (Standard deviations indicated by vertical lines). Hydrogen evolution determined by a chemical assay employing reduced methyl viologen as electron donor. Load, starting CrHydA1 protein

stock solution; FT, flow through; W1, first wash; W2, second wash; E, elution; P, ZnO particle suspension after elution; Negative control untreated ZnO.

The binding test was performed by mixing a stock solution of the CrHydA1 protein with a ZnO particle suspension under strict anaerobic conditions in order to adsorb the enzyme on the particle surface. Following the incubation, the fraction of CrHydA1 that still remained in solution was separated by centrifugation (supernatant denoted FT fraction), and the resulting pellet was washed twice with phosphate buffer to remove any residual unbound or weakly bound CrHydA1 from the ZnO (supernatant denoted W1 and W2). After this initial binding and wash procedure the hydrogenase functionalized ZnO particles were treated with an imidazole buffer, resulting in the release of any CrHydA1 enzymes binding *via* the his-tag, and the pellet was separated via centrifugation (supernatant denoted E, final pellet P). The enzyme content in each fraction was determined by studying the hydrogen evolution capacity of the respective supernatants as well as the final washed pellet in a chemical assay employing reduced methyl viologen (Figure 3). Additionally, the initial stock solution was assayed in parallel as well as untreated ZnO particles to provide a positive and negative control respectively (Figure 3, Load and ZnO). Unsurprisingly, high activity was observed in FT-fraction indicating incomplete binding of the enzyme to the ZnO particles, but following the second wash step the activity of the supernatant approached zero. Moreover, there was no significant H_2 production capacity observed for the imidazole containing elution fraction. Thus, once bound to the ZnO the enzyme does not appear to be spontaneously released into solution (Figure 3, FT – W2). In contrast, the pellet showed significantly higher hydrogenase activity than the W2 washing fraction (Figure 3, P). These observations clearly support the notion that CrHydA1 binds strongly to the ZnO, and that the binding appears to occur via electrostatic interactions rather than the hexa-histidine tag.

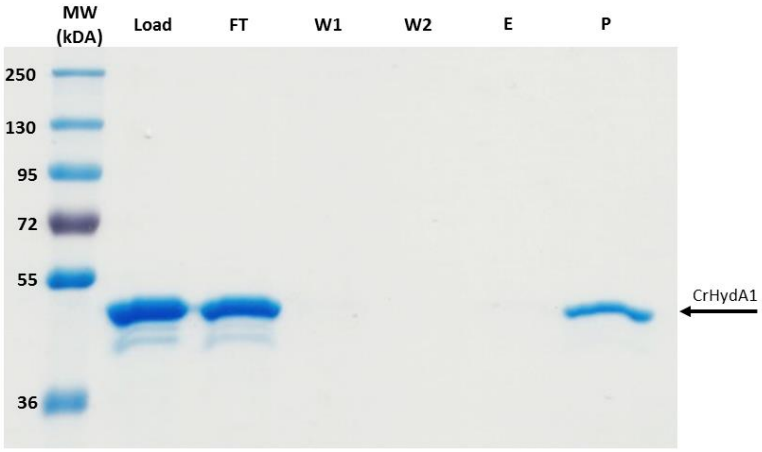

Figure 4. The adsorption of CrHydA1 to ZnO followed by SDS-PAGE gel. MW-molecular weight marker (Thermo Scientific PageRuler Plus Prestained Protein Ladder) Load, starting CrHydA1 protein stock solution; FT, flow through; W1, first wash; W2, second wash; E, elution; P, ZnO particle suspension after elution. The single 49 kDa protein band corresponds to the pure CrHydA1 protein.

The binding and molecular integrity, of the hydrogenase enzyme on ZnO particles was further verified by SDS-page gel analysis (Figure 4). The SDS-PAGE gels results clearly shows one single band in the final pellet (P) fraction which size corresponding to the CrHydA1 protein size (49 kDa), clearly showing that the enzyme remains intact upon binding.

In combination, these results show that CrHydA1 binds strongly to ZnO, without degradation of the enzyme. Moreover, as the combined activities of the initial flow through (Figure 3, FT) and the final pellet (Figure 3, P) is very close to the starting enzyme solution (Figure 3, positive control), ZnO binding does not seem to influence the activity of hydrogenase.

3.4 Performance of the Cu_2O-ZnO-hydrogenase electrode

Following the verification that CrHydA1 can adsorb onto ZnO in a stable fashion, hydrogenase functionalized electrodes (Cu_2O-ZnO-hydrogenase) were prepared *via* drop casting and their capacity for light driven H_2 production was analyzed. From previous experiment in section 3.2, we obtained a background photocurrent of 100 μA/cm^2 at a bias potential of 0.15 V *vs.* RHE from Cu_2O-ZnO-b electrode in the PEC test. In the presence of hydrogenase, the Cu_2O-ZnO-hydrogenase electrode rendered a tenfold increase in photocurrent, 0.8 mA/cm^2, as compared to the reference Cu_2O-ZnO-b electrode. Also, a positively-shifted onset potential (> 0.5 V vs RHE) was observed in Cu_2O-ZnO-hydrogenase electrode, suggesting that the Cu_2O-ZnO-hydrogenase system possesses the ability to perform HER at a lower bias potential (see Figure 5a). In order to verify H_2 production, an *in-situ* H_2 detection sensor was applied to directly trace the H_2 evolution signal, shown in Figure 5b. As described in section 3.2, no H_2 signal was detected for the reference Cu_2O-ZnO-b electrode. Excitingly, H_2 production was clearly observed during light irradiation (100 mW/cm^2) of the Cu_2O-ZnO-hydrogenase electrode. Eventually, 0.68 nmol of H_2 was obtained after accumulation for 200 s with light illumination, while 35.5 mC of charge went through the whole electrical circuit in the chronoamperometry measurement, rendering a Faradaic efficiency ca. 1 %. Although a low Faradaic efficiency was obtained probably due to the occurrence of non-productive side-reactions, these results strongly support the notion that the hydrogenase can be utilized as co-catalyst for H_2 production in Cu_2O-ZnO-hydrogenase electrodes.

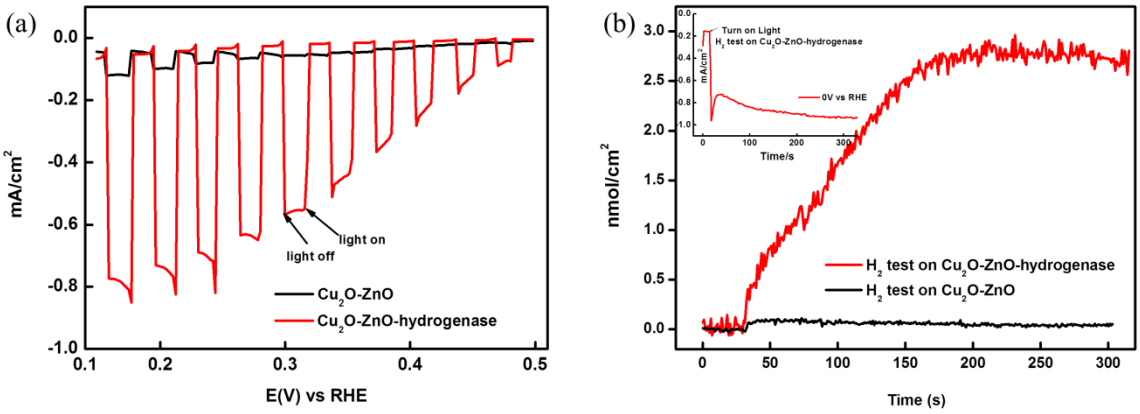

Figure 5. photoelectrochemical *J-V* test and H_2 evolution test. Cu_2O-ZnO in black line, Cu_2O-ZnO-hydrogenase in red line. a) linear scanning voltammetry (LSV) tests of different photoelectrodes with chopped light, b) H_2 production test; the inserted chronoamperometry test during H_2 evolution under 0 V *vs.* Reversed Hydrogen Electrode (RHE).

3.5 The formation of nano-sticks

In order to elucidate the side reaction occurring during the H_2 evolution, the morphology of the Cu_2O-ZnO and Cu_2O-ZnO-hydrogenase electrodes after the PEC test were investigated by SEM (Cu_2O-ZnO-a and Cu_2O-ZnO-hydrogenase electrodes-a), see Figure S6b and Figure 6, respectively. In the

absence of the hydrogenase, no significant change was observed between the Cu_2O-ZnO-b and Cu_2O-ZnO-a samples. However, nano-sticks with 0.5×0.1×0.1 μm size were piled-up on the surface of Cu_2O-ZnO-hydrogenase-a electrode. Zn, O, P, Fe and C element signals were further detected from the nano-sticks with EDX elements mapping analysis, but no Cu element signal was observed in the nano-sticks. This demonstrates that ZnO (Zn), phosphate buffer (P, no P element comprised inside hydrogenase) and hydrogenase (Fe, C) were involved in the formation of the nano-sticks. Thus, the low Faradaic efficiency and the decrease in H_2 production observed after 150-200 s is attributed to the loss of the protective ZnO layer due to formation of the observed nano-sticks, followed by fast degradation of the underlying Cu_2O electrode.

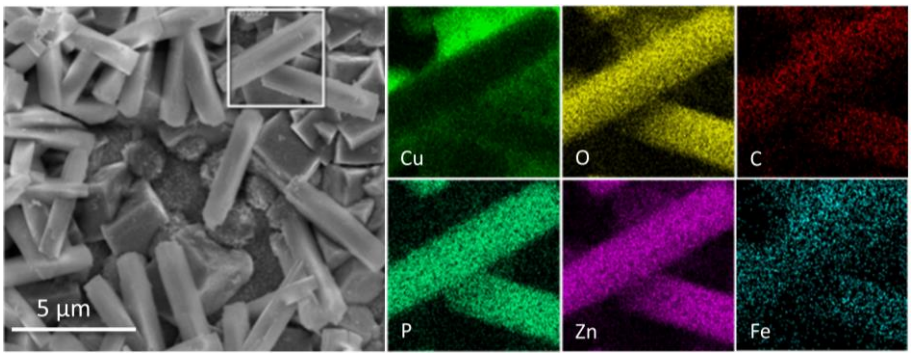

Figure 6. The SEM morphology of Cu_2O-ZnO-hydrogenase electrode (left) and Electron Disperse Spectroscopy (EDX) for the significant elements (right) after H_2 test.

4. Conclusion

In summary, we have shown the possibility of combining a low-cost inorganic p-Cu_2O semiconductor with a biological catalyst with high catalytic performance to fabricate a photocathode for light driven hydrogen evolution. In order to improve the stability of the bare Cu_2O, an easily applicable ZnO layer was introduced as protective layer by spin-coating method. The Cu_2O-ZnO-hydrogenase electrode was prepared by the spontaneous binding of the enzyme to the electrode surface via drop casting. Hydrogen evolution was observed only for the enzyme functionalized electrode. The low Faradaic efficiency and the formation of nano-sticks during operation indicate that additional work is required to generate stable systems. However, the mild potential requirement with neutral pH electrolyte for photo-driven HER showcases that the combination of low cost semiconductors, facile photoelectrode preparation methods, and noble metal free catalysts is a promising strategy for light driven proton reduction. In order to further improve the stability and performance of this kind of photocathode, it will require optimization of interfaces, electrode, material and immobilization of hydrogenase, all of which is currently explored.

Acknowledgements

We greatly acknowledge the financial support from following foundation: Stiftelsen Olle Engkvist Byggmästare (HT: 2015/456), The Swedish Energy Agency (111674-8), The Swedish Research Council, VR (GB: contract no. 621-2014- 5670), The Swedish Research Council for Environment, Agricultural Sciences and Spatial Planning, Formas (GB: contract no. 213-2014-880), the ERC (GB: StG contract no. 714102) the foundation Kung Karl XVI Gustafs 50-års-fond för vetenskap, miljö och teknik (GB) and the Wenner-Gren foundations (GB) are gratefully acknowledged for funding. Lei Tian also thanks China Scholarship Council (CSC) for the scholarship support. Dr. Charlène Esmieu is gratefully acknowledged for providing the $(Et_4N)_2[Fe_2(adt)(CO)_4(CN)_2]$ complex.

Appendix A. Supplementary data

The detailed procedures of [FeFe] hydrogenase CrHydA1 preparation; Photoelectrochemical tests of Cu_2O and Cu_2O-ZnO; SEM images of Cu_2O-a and Cu_2O-ZnO-a.

Reference

[1] A. Fujishima and K. Honda, Electrochemical photolysis of water at a semiconductor electrode, Nature 238 (1972), 37-38.

[2] A. Paracchino, V. Laporte, K. Sivula, M. Grätzel and E. Thimsen, Highly active oxide photocathode for photoelectrochemical water reduction, Nat. Mater. 10 (2011), 456-461.

[3] H. Tian, Molecular catalyst immobilized photocathodes for water/proton and carbon dioxide reduction, ChemSusChem 8 (2015), 3746-3759.

[4] S. N. Habisreutinger, L. Schmidt‐Mende and J. K. Stolarczyk, Photocatalytic reduction of CO_2 on TiO_2 and other semiconductors, Angew. Chem. Int. Ed. 52 (2013), 7372-7408.

[5] F. Li, K. Fan, B. Xu, E. Gabrielsson, Q. Daniel, L. Li and L. Sun, Organic dye-sensitized tandem photoelectrochemical cell for light driven total water splitting, J. Am. Chem. Soc. 137 (2015), 9153-9159.

[6] Y. Gao, X. Ding, J. Liu, L. Wang, Z. Lu, L. Li and L. Sun, Visible light driven water splitting in a molecular device with unprecedentedly high photocurrent density, J. Am. Chem. Soc. 135 (2013), 4219-4222.

[7] L. J. Antila, P. Ghamgosar, S. Maji, H. Tian, S. Ott and L. Hammarström, Dynamics and Photochemical H2 Evolution of Dye–NiO Photocathodes with a Biomimetic FeFe-Catalyst, ACS Energy Lett. 1 (2016), 1106-1111.

[8] P. B. Pati, L. Zhang, B. Philippe, R. Fernández‐Terán, S. Ahmadi, L. Tian, H. Rensmo, L. Hammarström and H. Tian, Insights into the Mechanism of a Covalently Linked Organic Dye–Cobaloxime Catalyst System for Dye‐Sensitized Solar Fuel Devices, ChemSusChem 10 (2017), 2480-2495.

[9] C. Y. Lee, H. S. Park, J. C. Fontecilla‐Camps and E. Reisner, Photoelectrochemical H_2 Evolution with a Hydrogenase Immobilized on a TiO_2‐Protected Silicon Electrode, Angew. Chem. Int. Ed. 55 (2016), 5971-5974.

[10] L. Li, L. Duan, F. Wen, C. Li, M. Wang, A. Hagfeldt and L. Sun, Visible light driven hydrogen production from a photo-active cathode based on a molecular catalyst and organic dye-sensitized p-type nanostructured NiO, Chem. Commun. 48 (2012), 988-990.

[11] Z. Ji, M. He, Z. Huang, U. Ozkan and Y. Wu, Photostable p-type dye-sensitized photoelectrochemical cells for water reduction, J. Am. Chem. Soc. 135 (2013), 11696-11699.

[12] K. Sivula, F. Le Formal and M. Grätzel, Solar water splitting: progress using hematite (α‐Fe_2O_3) photoelectrodes, ChemSusChem 4 (2011), 432-449.

[13] A. Kudo, K. Omori and H. Kato, A novel aqueous process for preparation of crystal form-controlled and highly crystalline $BiVO_4$ powder from layered vanadates at room temperature and its photocatalytic and photophysical properties, J. Am. Chem. Soc 121 (1999), 11459-11467.

[14] M. H. Lee, K. Takei, J. Zhang, R. Kapadia, M. Zheng, Y. Z. Chen, J. Nah, T. S. Matthews, Y. L. Chueh and J. W. Ager, p‐Type InP Nanopillar Photocathodes for Efficient Solar‐Driven Hydrogen Production, Angew. Chem. Int. Ed. 51 (2012), 10760-10764.

[15] P. Dai, W. Li, J. Xie, Y. He, J. Thorne, G. McMahon, J. Zhan and D. Wang, Forming buried junctions to enhance the photovoltage generated by cuprous oxide in aqueous solutions, Angew. Chem. Int. Ed. 53 (2014), 13493-13497.

[16] C. Li, T. Hisatomi, O. Watanabe, M. Nakabayashi, N. Shibata, K. Domen and J.-J. Delaunay, Positive onset potential and stability of Cu_2O-based photocathodes in water splitting by atomic layer deposition of a Ga_2O_3 buffer layer, Energy Environ. Sci. 8 (2015), 1493-1500.

[17] S. D. Tilley, M. Schreier, J. Azevedo, M. Stefik and M. Graetzel, Ruthenium oxide hydrogen evolution catalysis on composite cuprous oxide water‐splitting photocathodes, Adv. Funct. Mater. 24 (2014), 303-311.

[18] C. G. Morales‐Guio, L. Liardet, M. T. Mayer, S. D. Tilley, M. Grätzel and X. Hu, Photoelectrochemical Hydrogen Production in Alkaline Solutions Using Cu_2O Coated with Earth‐Abundant Hydrogen Evolution Catalysts, Angew. Chem. Int. Ed. 54 (2015), 664-667.

[19] W. Lubitz, H. Ogata, O. Rüdiger and E. Reijerse, Hydrogenases, Chem. Rev. 114 (2014), 4081-4148.

[20] M. Kato, T. Cardona, A. W. Rutherford and E. Reisner, Covalent Immobilization of Oriented Photosystem II on a Nanostructured Electrode for Solar Water Oxidation, J. Am. Chem. Soc. 135 (2013), 10610-10613.

[21] D. Mersch, C.-Y. Lee, J. Z. Zhang, K. Brinkert, J. C. Fontecilla-Camps, A. W. Rutherford and E. Reisner, Wiring of Photosystem II to Hydrogenase for Photoelectrochemical Water Splitting, J. Am. Chem. Soc. 137 (2015), 8541-8549.

[22] A. A. Oughli, F. Conzuelo, M. Winkler, T. Happe, W. Lubitz, W. Schuhmann, O. Rüdiger and N. Plumeré, A Redox Hydrogel Protects the O2-Sensitive [FeFe]-Hydrogenase from Chlamydomonas reinhardtii from Oxidative Damage, Angew. Chem., Int. Ed. Engl. 54 (2015), 12329-12333.

[23] N. Plumeré, O. Rüdiger, A. A. Oughli, R. Williams, J. Vivekananthan, S. Pöller, W. Schuhmann and W. Lubitz, A redox hydrogel protects hydrogenase from high-potential deactivation and oxygen damage, Nat Chem 6 (2014), 822-827.

[24] M. Hambourger, M. Gervaldo, D. Svedruzic, P. W. King, D. Gust, M. Ghirardi, A. L. Moore and T. A. Moore, [FeFe]-Hydrogenase-Catalyzed H2 Production in a Photoelectrochemical Biofuel Cell, J. Am. Chem. Soc. 130 (2008), 2015-2022.

[25] L. Loiseau, S. Ollagnier-de Choudens, D. Lascoux, E. Forest, M. Fontecave and F. Barras, Analysis of the Heteromeric CsdA-CsdE Cysteine Desulfurase, Assisting Fe-S Cluster Biogenesis in Escherichia coli, J. Biol. Chem. 280 (2005), 26760-26769.

[26] H. Li and T. B. Rauchfuss, Iron Carbonyl Sulfides, Formaldehyde, and Amines Condense To Give the Proposed Azadithiolate Cofactor of the Fe-Only Hydrogenases, J. Am. Chem. Soc. 124 (2002), 726-727.

[27] J. Esselborn, C. Lambertz, A. Adamska-Venkatesh, T. Simmons, G. Berggren, J. Noth, J. Siebel, A. Hemschemeier, V. Artero, E. Reijerse, M. Fontecave, W. Lubitz and T. Happe, Spontaneous activation of [FeFe]-hydrogenases by an inorganic [2Fe] active site mimic, Nat. Chem. Biol. 9 (2013), 607-609.

[28] D. W. Mulder, D. O. Ortillo, D. J. Gardenghi, A. V. Naumov, S. S. Ruebush, R. K. Szilagyi, B. Huynh, J. B. Broderick and J. W. Peters, Activation of HydAÎ”EFG Requires a Preformed [4Fe-4S] Cluster, Biochemistry 48 (2009), 6240-6248.

[29] G. Berggren, A. Adamska, C. Lambertz, T. R. Simmons, J. Esselborn, M. Atta, S. Gambarelli, J. M. Mouesca, E. Reijerse, W. Lubitz, T. Happe, V. Artero and M. Fontecave, Biomimetic assembly and activation of [FeFe]-hydrogenases, Nature 499 (2013), 66-69.

[30] A. Paracchino, J. C. Brauer, J.-E. Moser, E. Thimsen and M. Graetzel, Synthesis and Characterization of High-Photoactivity Electrodeposited Cu, J. Phys. Chem. C 116 (2012), 7341–7350.

[31] X. Shi, L. Cai, M. Ma, X. Zheng and J. H. Park, General Characterization Methods for Photoelectrochemical Cells for Solar Water Splitting, ChemSusChem 8 (2015), 3192-3203.

Supporting information for

Hydrogen evolution by a photoelectrochemical cell based on a Cu_2O-ZnO-[FeFe] hydrogenase electrode

Lei Tian[1, †], Brigitta Németh[2, †], Gustav Berggren[2,*], Haining Tian[1,*]

1. *Physical Chemistry, Department of Chemistry – Ångström Laboratory, Uppsala University, BOX 523, 75120, Uppsala, Sweden. E-mail: haining.tian@kemi.uu.se*
2. *Molecular Biomimetics, Department of Chemistry – Ångström Laboratory, Uppsala University, BOX 523, 75120, Uppsala, Sweden. E-mail: gustav.berggren@kemi.uu.se*

† These authors contribute equally

Heterologous expression and purification of CrHydANHis

The CrHydA1 gene encoding expression vector was kindly provided by Marc Fontecave. BL21(DE3) competent cells were transformed with pet DUET-CrHydA1 expression vector and the positive clones were selected based on ampicillin resistance. Large scale expression was performed in LB medium complemented with 25 mM potassium phosphate buffer and 5% glucose[1], when the culture reached OD600 0.4-0.6, the cultures were transferred to 16 °C and the protein expression was induced via 1 mM IPTG. After 12-16 hours the cells were harvested by centrifugation, and the cell paste was resuspended in 100 mM HEPES pH 7.4, 300 mM NaCl, 10 mM $MgCl_2$, 5% glycerol. The suspension was centrifuged and the cell paste was immediately frozen in liquid nitrogen, and kept at -80 °C until further usage. The cell paste was thawed and resuspended in a presence of lysozyme, DNAse, and RNAse in 100 mM HEPES pH 7.4, 300 mM NaCl, 10 mM $MgCl_2$, 5% glycerol, and freezed-thawed at least 3 times in liquid nitrogen. The semi-lysed cells were broken by discontinous sonication and the unbroken cells, inclusion bodies and the membrane fraction was separated from the soluble fraction via ultracentrifugation. The UC supernatant was loaded onto Ni-NTA (HisTrap) which was previously equilibrated with 100 mM HEPES pH 7.4, 300 mM NaCl, 10 mM $MgCl_2$, 5% glycerol. The column was extensively washed with equilibration buffer until the UV absorbance reached the baseline. To eliminate the unspecifically bounded proteins the column was washed with 100 mM HEPES pH 7.4, 300 mM NaCl, 10 mM $MgCl_2$, 5% glycerol and 50 mM imidazole containing buffer for 3-5 CV, and when the absorbance reached the baseline again, 10 CV 10-100 % linear gradient elution was performed (elution buffer composition: 100 mM HEPES pH 7.4, 300 mM NaCl, 10 mM $MgCl_2$, 5% glycerol and 500 mM imidazole). The imidazole was removed and the protein was concentrated via 30 kDa centricon (Merck). The his-tagged CrHydA1 was migrating on the gel as a single band.

Demetallization and size exclusion chromatography

The oxidized FeS cluster residues were removed via chelation (10 mM EDTA) in a presence of reducing agent (20 mM Na-dithionite) under strict anaerobic conditions. The protein solution was incubated for 1-2 hours at 4°C under strict anaerobic conditions. To separate the chelated Fe atoms from the apo protein, the protein was gel filtrated via Superdex200. The column was equilibrated with 100 mM Tris-HCl pH 8.0, 300 mM NaCl, 10 mM $MgCl_2$ and 5% glycerol.

In vitro Reconstitution

The iron-sulfur cluster reconstitution was performed under strict anaerobic conditions in MBRAUN glovebox. The protein sample was incubated 1-2 hours at 4°C under strict anaerobic conditions, and then it was incubated with tenfold molar excess of DTT for 10-15 minutes at room temperature. The DTT incubation was followed by the addition of sixfold molar excess of ferrous ammonium sulfate and sixfold molar excess of L-cysteine. The reconstitution reaction was initiated by the addition of 1-2 % molar equivalent of CsdA (Cysteine desulfurilase from *E.coli*). The reaction was followed by UV/Visible spectroscopy and when the reaction reached the platue, it was stopped by desalting via NAP25 columns. The NAP25 elution fractions were collected and concentrated via 30 kDa centricon. The proteins were aliquoted into PCR tubes and the PCR tubes were transferred into gastight serum vials, and the serum vials were immediately frozen in liquid nitrogen. The reconstituted proteins were kept at -80°C until further usage.

EPR sample preparation

The 200 µl 200 µM reconstituted CrHydA was incubated in a presence of 20 equivalent sodium dithionite until the oxidized iron-sulfur cluster peak disappeared in the UV/Vis spectrum. The fully reduced protein solution was transferred into an EPR tube and flash frozen immediately outside the glovebox. The EPR sample was kept on liquid nitrogen until further usage.

In vitro maturation

The reconstituted proteins were incubated with twentyfold molar excess of sodium dithionite and twelvefold molar excess of adt complex for 90 minutes at room temperature in the darkness under strict anaerobic conditions in the glovebox. After 90 minutes the maturation reaction was loaded onto a NAP25 desalting column, and the elution fractions were collected and concentrated via 30 kDa centricon.

Hydrogen evolution assays

The hydrogen evolution assay was performed based on reported method[2] in which 10 mM methyl viologen and 20 mM sodium dithionite as electron donor was used. In our hands, 1µg matured CrHydA1 in 1800 µl potassium phosphate buffer, oxidized methyl viologen and 1% Triton X-100 was transferred into a 8 ml serum vial which was closed inside the glovebox. The reaction mixture was transferred to 28 °C and let the reaction equilibrated 5-10 minutes. The reaction has been started with the addition of 200 µl 1 M sodium dithionite solution, and the hydrogen production was measured by gas-chromatography after 10 minutes.

Photoelectrochemical measurements

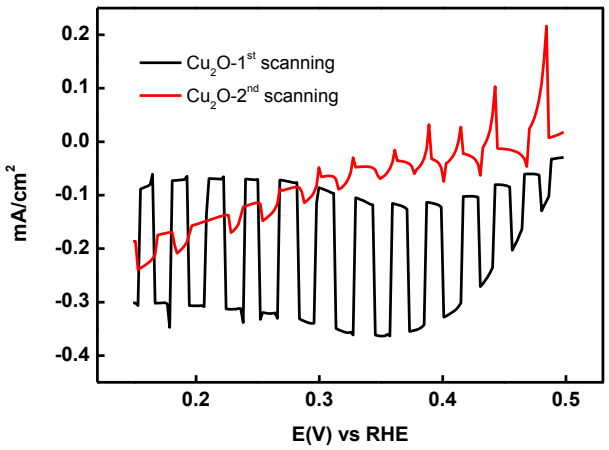

Figure S1. photoelectrochemical *J-V* tests by the chopped linear scanning voltammetry (LSV) method, the first scanning Cu_2O-1; the second scanning Cu_2O-2.

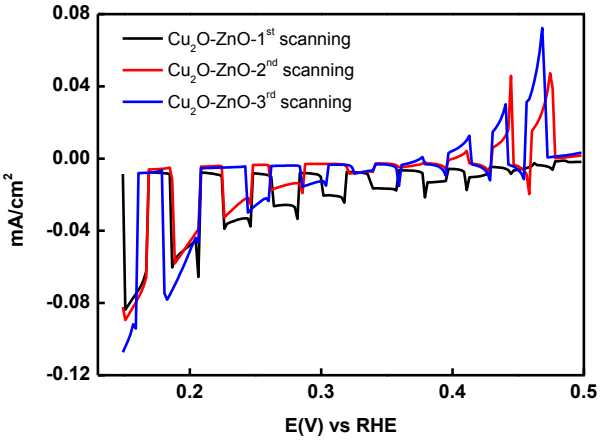

Figure S2. photoelectrochemical *J-V* tests by the chopped linear scanning voltammetry (LSV) method, the first scanning Cu_2O-ZnO-1; the second scanning Cu_2O-ZnO-2; the third scanning Cu_2O-ZnO-3.

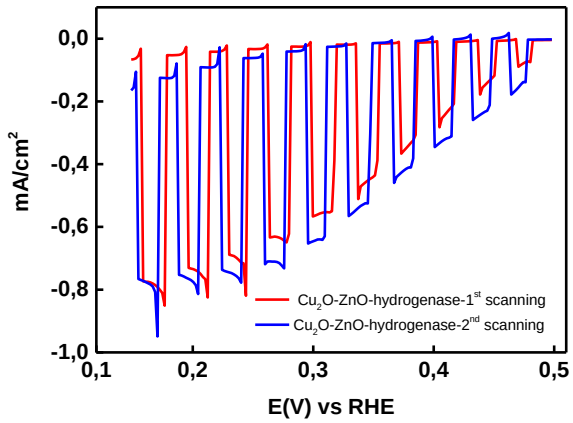

Figure S3. photoelectrochemical *J-V* tests by the chopped linear scanning voltammetry (LSV) method, the first scanning Cu_2O-ZnO-hydrogenase-1; the second scanning Cu_2O-ZnO-hydrogenase-2.

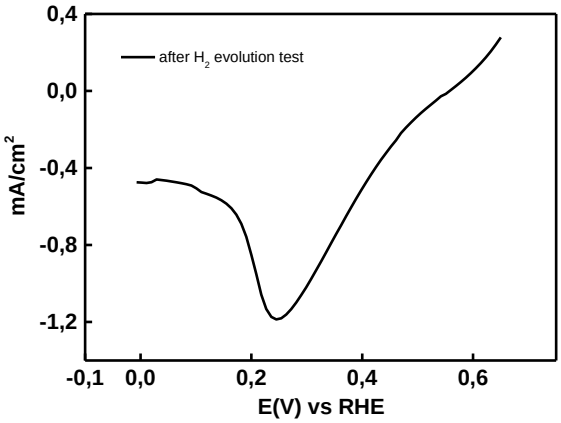

Figure S4. photoelectrochemical *J-V* test by the chopped linear scanning voltammetry (LSV) method, the Cu_2O-ZnO-hydrogenase sample after H_2 evolution test.

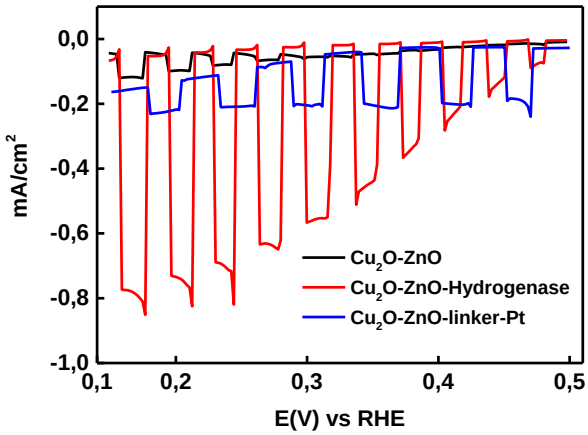

Figure S5. photoelectrochemical *J-V* test and H_2 evolution test. Cu_2O-ZnO in black line, Cu_2O-ZnO-hydrogenase in red line and Cu_2O-ZnO-linker-Pt in blue line.

The (3-Aminopropyl)trimethoxysilane was chosen as the linker in the experiment and 5 nm Platinum (Pt) nanoparticles was prepared based on the reference[3]. The linking experiment was performed based on the reference[4].

SEM morphology

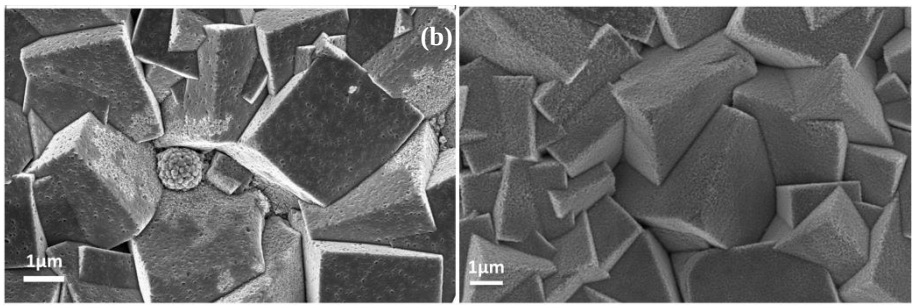

Figure S6. the SEM morphology of the electrodes after H2 test, a) Cu_2O-a; b) Cu_2O-ZnO-a.

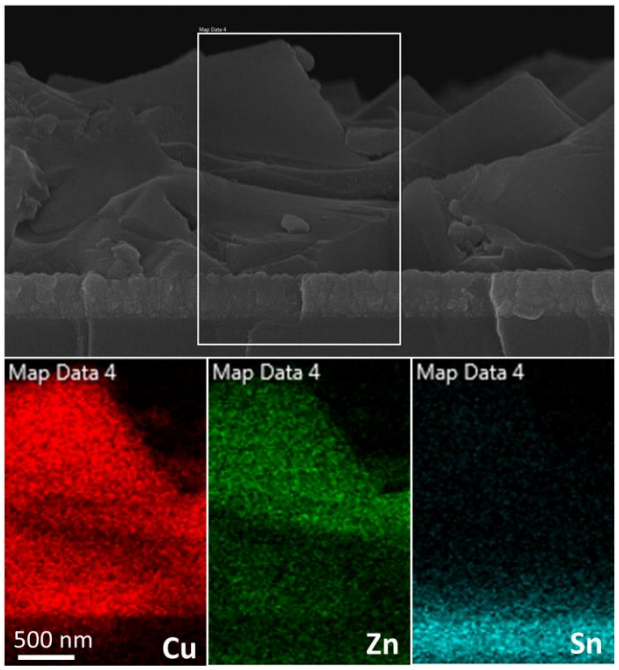

Figure S7. The SEM morphology in crossing section of of Cu_2O-ZnO-b, and the corresponding EDX elements mapping analysis.

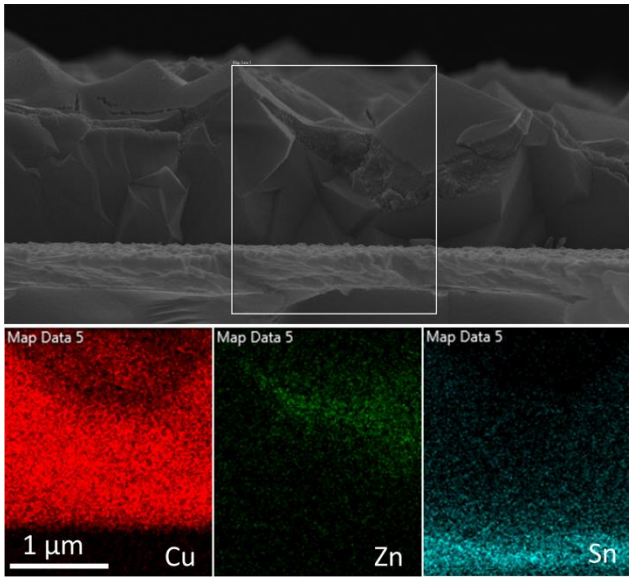

Figure S8. The SEM morphology in crossing section of Cu_2O-ZnO-b with 2 layer ZnO coating, and the corresponding EDX elements mapping analysis. 2 layer ZnO coating means the one extra ZnO layer deposition on the Cu_2O-ZnO-b film was deposited by the same procedure.

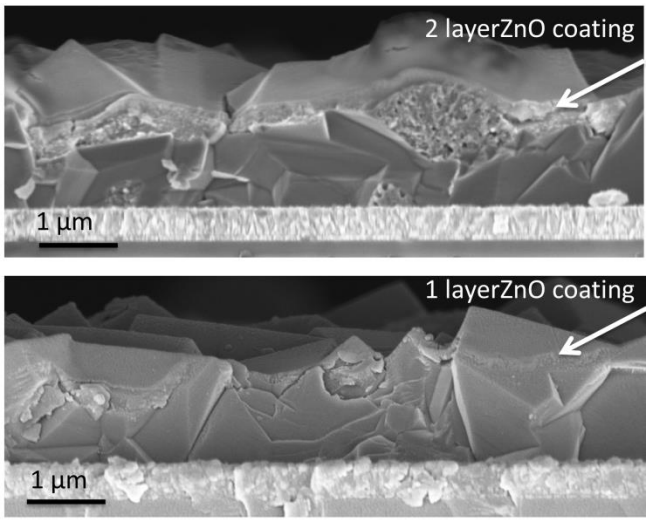

Figure S9. The SEM morphology in crossing section of Cu_2O-ZnO-b (with 1 layer ZnO coating), and Cu_2O-ZnO-b with 2 layer ZnO coating. The thicker ZnO layer can be observed from 2 layer ZnO coating sample.

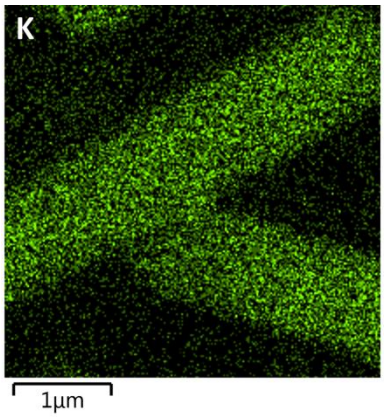

Figure S10. The EDX element mapping analysis of K on the nano-sticks of Figure 6.

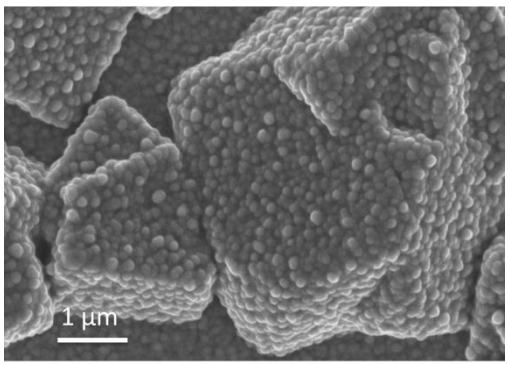

Figure S11. The SEM morphology of Cu_2O-TiO_2 sample. Atomic layer deposition (ALD) method was used to deposit TiO_2 on the Cu_2O surface. The TiO_2 nanoparticles was found on the Cu_2O surface without conformal coating. It may result from the bad affinity between Cu_2O and TiO_2.

Small-angle X-ray diffraction

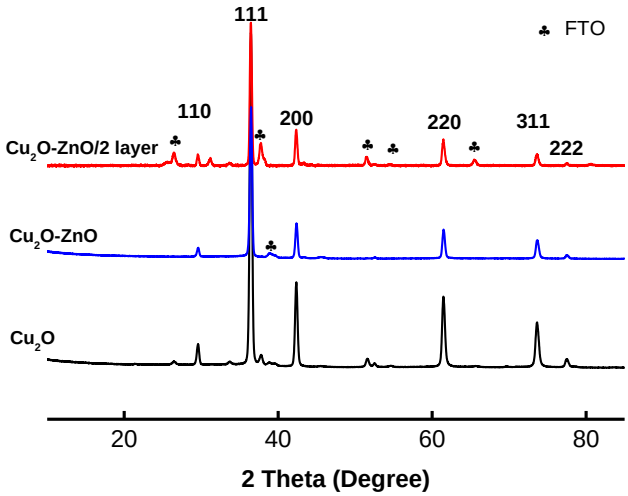

Figure S12. Small-angle X-ray diffraction curves of Cu_2O-ZnO/ (2 layer ZnO/ red line), Cu_2O-ZnO (1 layer ZnO/blue line) and Cu_2O (black line). No XRD peaks can be ascribed to the formation of crystallized ZnO even in the Cu_2O-ZnO/2 layer sample with more fraction of ZnO deposited, proving the amorphous structure of ZnO mentioned in the main text.

Reference

[1] D. W. Mulder, D. O. Ortillo, D. J. Gardenghi, A. V. Naumov, S. S. Ruebush, R. K. Szilagyi, B. Huynh, J. B. Broderick and J. W. Peters, Activation of HydAΔEFG requires a preformed [4Fe-4S] cluster, Biochemistry 48 (2009), 6240-6248.

[2] J. Esselborn, C. Lambertz, A. Adamska-Venkatesh, T. Simmons, G. Berggren, J. Noth, J. Siebel, A. Hemschemeier, V. Artero and E. Reijerse, Spontaneous activation of [FeFe]-hydrogenases by an inorganic [2Fe] active site mimic, Nat. Chem. Biol. 9 (2013), 607-609.

[3] N. C. Bigall, T. Härtling, M. Klose, P. Simon, L. M. Eng and A. Eychmüller, Monodisperse platinum nanospheres with adjustable diameters from 10 to 100 nm: synthesis and distinct optical properties, Nano Lett. 8 (2008), 4588-4592.

[4] K. C. Grabar, R. G. Freeman, M. B. Hommer and M. J. Natan, Preparation and characterization of Au colloid monolayers, Anal. Chem. 67 (1995), 735-743.